Attenuation analysis of cross-hole data generated during hydraulic fracturing

Bharath Shekar & Ilya Tsvankin
Center for Wave Phenomena, Colorado School of Mines, Golden CO 80401

ABSTRACT
Measurements of attenuation anisotropy can provide valuable information for reservoir characterization and monitoring. Here, we analyze a cross-hole data set generated by perforation shots fired in a horizontal borehole to induce hydraulic fracturing in a tight gas reservoir. The spectral-ratio method is applied to pairs of traces to set up a system of equations for directionally-dependent effective attenuation. The anisotropic attenuation coefficient is expanded in a quadratic function of the polar and azimuthal angles of the source-receiver line. The coefficients of this polynomial are found separately for each stage of perforation shots. Although the inversion provides clear evidence of attenuation anisotropy, the narrow range of propagation directions impairs the accuracy of anisotropy analysis. The observed variations of the attenuation coefficient between different perforation stages may be related to changes in the medium due to hydraulic fracturing and stimulation.

Key words: anisotropy, attenuation, cross-hole, tight gas, hydraulic stimulation

1 INTRODUCTION

Attenuation of seismic waves is sensitive to the physical properties of the subsurface and has been observed in vertical seismic profiling (VSP) and reflection data. De et al. (1994) report measurements of the P- and S-wave quality factors from VSP surveys and sonic logs. Maultzsch et al. (2007) evaluate P-wave azimuthal attenuation anisotropy from 3D VSP data acquired over a fractured hydrocarbon reservoir and infer fracture directions from attenuation analysis. Barnes (2010) estimates shear-wave attenuation using anisotropic full-waveform inversion of offshore VSP data acquired over a gas reservoir. Attenuation anisotropy has also been observed in P-wave reflection data (Clark et al., 2009; Vasconcelos and Jenner, 2005).

Seismic attenuation is most commonly measured using the spectral-ratio method. Zhu et al. (2007) extend the spectral-ratio method to anisotropic media and apply it to physical-modeling data acquired for a transversely isotropic (TI) sample. Other techniques proposed to measure attenuation include the instantaneous-frequency (Dasios et al., 2001), and frequency-shift methods (Quan and Harris, 1997). These algortihms, however, require a broad range of frequencies and knowledge of the source spectrum, which is difficult to estimate in practice. In contrast, computing spectral ratios helps eliminate the source spectrum and can be used to obtain accurate effective and interval attenuation coefficients in layered anisotropic media (Behura and Tsvankin, 2009a; Shekar and Tsvankin, 2010).

Here, we present a case study with cross-hole data generated by perforation shots in a horizontal borehole and recorded in a vertical borehole. The spectral-ratio method applied to all pairs of traces yields a system of equations for the anisotropic attenuation coefficient. Since the acquisition aperture is narrow, we represent the directional dependence of the attenuation coefficient as a quadratic polynomial of the polar and azimuthal angles. The inversion results show that taking attenuation anisotropy into account reduces the data misfit and reveals changes in the attenuation coefficient between perforation stages. Interpretation of the attenuation measurements is not straightforward, but it provides indications of temporal changes related to hydraulic fracturing.

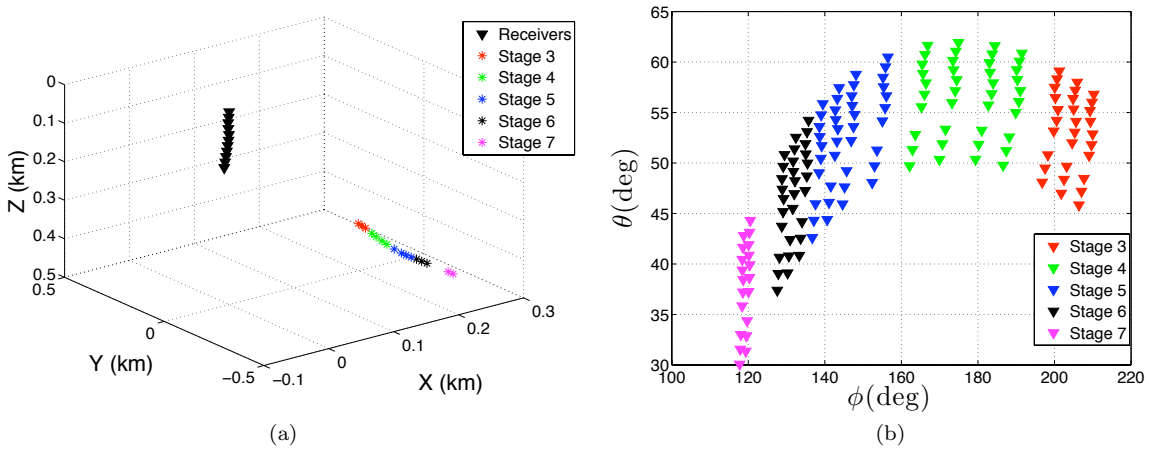

(a) (b)

Figure 1. Acquisition geometry of the experiment; the x-axis points east. The shots in a horizontal borehole are denoted by stars, with different colors corresponding to different stages. The receivers in a vertical borehole are denoted by black triangles. The shot and receiver positions are plotted (a) in the Cartesian coordinates, and (b) as functions of the polar (θ) and azimuthal (ϕ) angles of the source-receiver line.

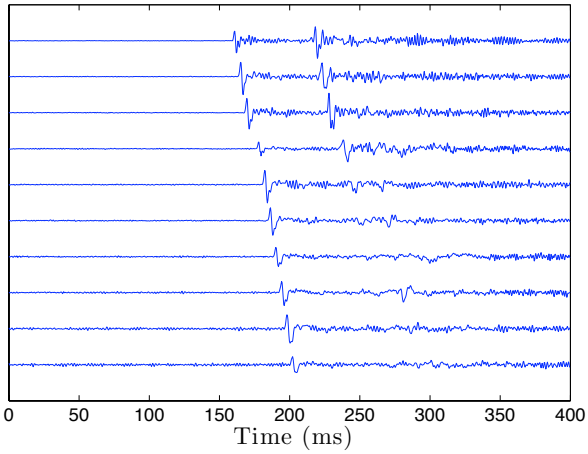

Figure 2. Typical shot gather from the data set. The first arrivals with a linear moveout are the direct P-waves. The recorded displacement components were rotated to enhance P-wave energy.

2 METHODOLOGY

The data used in our study were generated in a tight-gas reservoir by perforation shots fired at regular intervals in a horizontal borehole. The wavefield was recorded by 10 multicomponent receivers placed at different depths in a vertical (monitor) borehole (Figure 1). The perforation shots were grouped into successive "stages," as borehole perforations at each stage were followed by hydraulic stimulation of the perforation-induced fractures.

Multicomponent shot gathers were rotated to maximize the energy of the direct P-waves (Figure 2). After picking the P-wave arrivals, we applied a tapered cosine window around the signal. The amplitude spectra of P-waves excited by one of the perforation shots and recorded at two geophones are shown in Figure 3. The spectrum of the event with the longer raypath is shifted towards lower frequencies, which indicates the influence of attenuation.

The ray-theoretical frequency-domain amplitude of the P-wave propagating between the ith source and the jth receiver in a homogeneous, anisotropic, attenuative medium can be written as

$$|A_{ij}| = S_i(\omega)\, \mathcal{G}_{ij}\, e^{-k^I_{ij}\, x_{ij}}, \tag{1}$$

where $S_i(\omega)$ represents the source spectrum and $\mathcal{G}_{ij}$ (assumed to be frequency-independent) incorporates the geometrical spreading and transmission coefficients along the raypath and the source/receiver directivity function. The coefficient k^I_{ij} is the imaginary part of the P-wave *group* wavenumber along the raypath for the source-receiver pair ij, and x_{ij} is the raypath length. According to the results of Behura and Tsvankin (2009b), equation 1 can be rewritten in terms of the normalized *phase* attenuation coefficient $\mathcal{A}_{ij}$ in the following way:

$$|A_{ij}| = S_i(\omega)\, \mathcal{G}_{ij}\, e^{-\omega\, \mathcal{A}_{ij}\, t_{ij}}, \tag{2}$$

where ω is the angular frequency and t_{ij} is the traveltime. The coefficient $\mathcal{A}_{ij}$ should be obtained for the phase direction corresponding to the source-receiver line.

Since the perforation shots were not timed, the times picked on the shot gathers (e.g., in Figure 2) do not correspond to the actual traveltimes t_{ij} between the sources and receivers. Grechka and Duchkov (2011) estimate the origin times of the perforation shots by building homogeneous anisotropic velocity models. However, they show that the origin times can be obtained with reasonable accuracy for a homogeneous

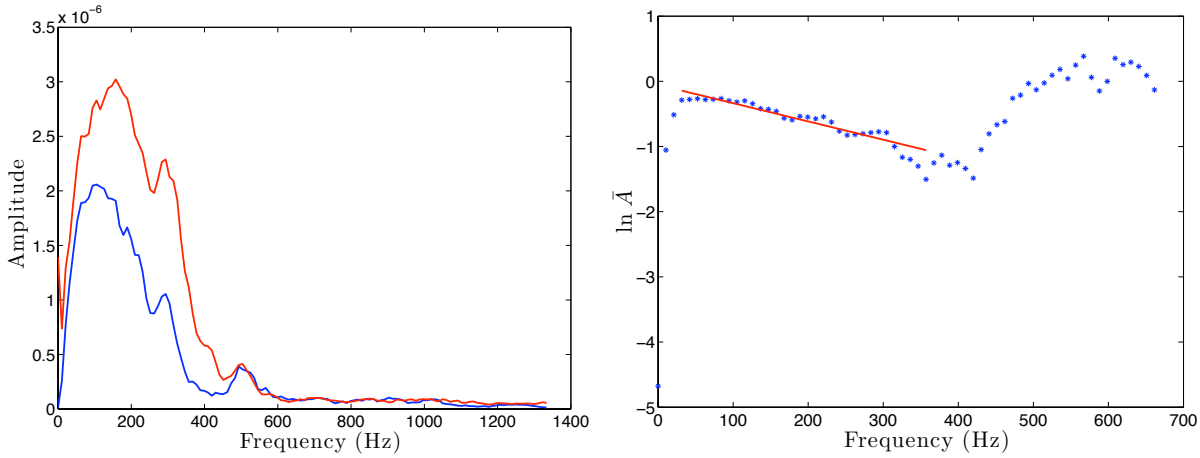

Figure 3. (a) Amplitude spectra of two P-wave arrivals excited by one of the shots in stage 3 and recorded by the shallowest (red curve) and deepest (blue curve) geophones. (b) The logarithmic spectral ratio of the amplitude spectra (blue stars) and the best-fit straight line (red) in the selected frequency band.

isotropic medium. Hence, we estimate the velocity of the direct P-waves from the slope of the vertical moveout observed in the receiver array under the assumption that the medium is isotropic and homogeneous (see Figure 2).

The logarithmic spectral ratio for two P-wave arrivals excited by the ith source and recorded by receivers j and k has the form:

$$\ln \bar{A} = \ln \left| \frac{A_{ij}}{A_{ik}} \right| = \ln \mathcal{G} - \omega\, s_{ijk}, \tag{3}$$

$$s_{ijk} = \mathcal{A}_{ij}\, t_{ij} - \mathcal{A}_{ik}\, t_{ik}, \tag{4}$$

where $\mathcal{G} = \mathcal{G}_{ij}/\mathcal{G}_{ik}$ is assumed to be frequency-independent. Note that the source spectrum in equation 3 is eliminated. Hence, the slope of the logarithmic spectral ratio for two source-receiver pairs yields the quantity s_{ijk}, which depends on the corresponding phase attenuation coefficients.

The spectral ratio computed for the two amplitude spectra from Figure 3a is displayed in Figure 3b. The bandwidth used in the spectral-ratio method has to be chosen in a frequency range where the signal-to-noise ratio is sufficiently high (e.g., $30-350$ Hz in Figure 3a). To obtain a robust estimate of s_{ijk}, we employ the iteratively reweighted least-squares method (Scales and Gersztenkorn, 1988; Aster et al., 2005).

In homogeneous isotropic media, the attenuation coefficient $\mathcal{A}$ is constant for all source-receiver pairs. If the medium is anisotropic, the coefficient $\mathcal{A}$ varies with the orientation of the source-receiver line. By treating all attenuation coefficients as independent quantities, we can set up a system of linear equations for each stage. For example, the third stage includes three shots and 10 receivers, and the system of linear equations that includes the results for all source-receiver pairs is

$$s_{ijk} = \mathcal{A}_{ij}\, t_{ij} - \mathcal{A}_{ik}\, t_{ik};\ 1 \le i \le 3,\ 1 \le j < k \le 10, \tag{5}$$

where, as before, the index i denotes the source, while j and k denote the receivers.

Linear system 5 is overdetermined (there are 135 equations for 30 unknowns), but ill-conditioned due to closely spaced receivers and small differences between the arrival times. Hence, the attenuation coefficient along each raypath cannot be resolved individually. Note that the above analysis assumes that the medium is homogeneous. In the presence of heterogeneity, the recovered attenuation coefficients represent effective quantities for each source-receiver pair.

To reduce the number of unknowns but still honor attenuation anisotropy, we need to express attenuation coefficients as functions of angle. Zhu and Tsvankin (2006, 2007) obtain approximate phase attenuation coefficients of P- and S-waves in homogeneous TI and orthorhombic media in terms of Thomsen-style attenuation-anisotropy parameters. Their expression for the P-wave phase attenuation coefficient in orthorhombic media with the symmetry planes aligned with the Cartesian coordinate planes is

$$\mathcal{A}_P(\theta,\phi) = \mathcal{A}_{P0}[1 + \delta_Q(\phi)\, \sin^2\theta \cos^2\theta + \epsilon_Q(\phi) \sin^4\theta], \tag{6}$$

where $\mathcal{A}_{P0}$ is the vertical attenuation coefficient, θ is the polar angle, ϕ is the azimuth with respect to the x_1-axis, and

$$\delta_Q(\phi) = \delta_Q^{(1)} \sin^2\phi + \delta_Q^{(2)} \cos^2\phi, \tag{7}$$

$$\epsilon_Q(\phi) = \epsilon_Q^{(1)} \sin^4\phi + \epsilon_Q^{(2)} \cos^4\phi + (2\epsilon_Q^{(2)} + \delta_Q^{(3)}) \sin^2\phi \cos^2\phi. \tag{8}$$

The attenuation-anisotropy parameters $\delta_Q^{(1,2,3)}$ and $\epsilon_Q^{(1,2)}$ are defined in Zhu and Tsvankin (2007).

Since equations 6–8 are derived in the linearized weak-anisotropy approximation, the phase angle can be replaced with the group angle of the source-receiver direction (see Figure 1b). However, due to the limited angular coverage and absence of near-vertical raypaths, the attenuation-anisotropy parameters cannot be resolved with sufficient accuracy. Therefore, we represent $\mathcal{A}_{ij}$ by a second-order polynomial of the polar (θ_{ij}) and azimuthal (ϕ_{ij}) angles of the corresponding source-receiver direction (Figure 1b):

$$\mathcal{A}_{ij} = A + B\,\tilde{\theta}_{ij} + C\,\tilde{\theta}_{ij}^2 + D\,\tilde{\phi}_{ij} + E\,\tilde{\phi}_{ij}^2 + F\,\tilde{\theta}_{ij}\,\tilde{\phi}_{ij}, \tag{9}$$

$$\tilde{\theta}_{ij} = \theta_{ij} - \theta_c,\ \tilde{\phi}_{ij} = \phi_{ij} - \phi_c, \tag{10}$$

where the mean values of the polar and azimuthal angles for a given stage (corresponding to the "central ray") are denoted by θ_c and ϕ_c, respectively. Substituting equation 9 into equation 5, we obtain the following system of linear equations:

$$\begin{aligned} s_{ijk} &= A\,(t_{ij} - t_{ik}) + B\,(t_{ij}\,\tilde{\theta}_{ij} - t_{ik}\,\tilde{\theta}_{ik}) \\ &+ C\,(t_{ij}\,\tilde{\theta}_{ij}^2 - t_{ik}\,\tilde{\theta}_{ik}^2) + D\,(t_{ij}\,\tilde{\phi}_{ij} - t_{ik}\,\tilde{\phi}_{ik}) \\ &+ E\,(t_{ij}\,\tilde{\phi}_{ij}^2 - t_{ik}\,\tilde{\phi}_{ik}^2) + F\,(t_{ij}\,\tilde{\theta}_{ij}\,\tilde{\phi}_{ij} - t_{ik}\,\tilde{\theta}_{ik}\,\tilde{\phi}_{ik}). \end{aligned} \tag{11}$$

System of equations 11 can be represented in matrix form,

$$\mathbf{S} = \mathbf{G}\mathbf{m}, \tag{12}$$

$$\mathbf{m} = [A\ B\ C\ D\ E\ F]^{\mathrm{T}}, \tag{13}$$

where $\mathbf{S}$ is the vector formed by the elements s_{ijk} and $\mathbf{G}$ is the matrix formed by the terms multiplied with elements of $\mathbf{m}$. The vector $\mathbf{m}$, which quantifies attenuation anisotropy, is estimated for each stage separately. Note that $\mathbf{m}$ could vary from stage to stage due to hydraulic stimulation and the fact that source-receiver raypaths for each stage probe different volumes of rock.

By expressing the attenuation coefficient as a polynomial function of angle, the number of unknown parameters for each stage reduces to six. The vector $\mathbf{m}$ is found as the least-squares solution that minimizes the data misfit,

$$\psi = ||\mathbf{G}\mathbf{m} - \mathbf{S}||^2. \tag{14}$$

Because not all elements of $\mathbf{m}$ are well constrained by the data, we perform best-subset regression (Draper and Smith, 1981). We consider models with all possible combinations of the elements of $\mathbf{m}$ (equation 13), and compute the root-mean-square (rms) error and the p-values for the coefficients from Student's t-distribution. The p-value is a measure of the probability that the estimated coefficient is zero. We reject models with coefficients whose p-values are greater than 0.10 and select the model with the least value of the rms error as the solution. Assuming isotropic (angle-independent) attenuation results in a higher rms error, so taking anisotropy into account is essential to fit the data.

3 INVERSION RESULTS

The best-fit inverted coefficients and their standard deviations are listed in Table 1. Directional dependence of attenuation is non-negligible, with polar anisotropy more pronounced than azimuthal anisotropy. The only exception is stage 5, which exhibits relatively weak attenuation anisotropy. The attenuation coefficient for stage 6 is substantially lower than that for the other stages, most likely due to the influence of heterogeneity and/or measurement errors.

The analytic attenuation coefficient in equation 6 can be expanded in a Taylor series around the mean values of the polar (θ) and azimuthal (ϕ) angles for each stage. If the orientation of the symmetry planes is known, the six polynomial coefficients in equation 7 can be used to uniquely determine all six Thomsen-style parameters. However, due to the trade-offs between the coefficients of the polynomial, the attenuation-anisotropy parameters cannot be resolved individually. Physically, the range of the polar and azimuthal angles in the experiment is too narrow to constrain $\mathcal{A}_{P0}$, $\delta_Q^{(1,2,3)}$, and $\epsilon_Q^{(1,2)}$.

It is essential to evaluate the sensitivity of the inversion results to uncertainties in the origin times. We added 100 realizations of Guassian noise with a standard deviation of 20 time samples to the origin times and estimated the coefficients in equation 9 for each of these realizations. The mean values and standard deviations of the elements of the vector $\mathbf{m}$ are listed in Table 2. Clearly, the inversion results are weakly influenced by errors in the origin times. In fact, comparison of Tables 1 and 2 shows that the inverted attenuation coefficient is more sensitive to noise in the spectral-ratio estimates.

The mean values and standard deviations of the attenuation coefficients $\mathcal{A}_P$ for all source-receiver pairs are shown in spherical coordinates in Figure 4. The mean value of the attenuation coefficient decreases with the stage number. This variation in attenuation is likely related to the changes in the medium due to hydraulic fracturing and pumping of fluids through the rock volume.

4 CONCLUSIONS

We introduced a methodology for estimating the directionally dependent P-wave attenuation coefficient from cross-hole data acquired for a relatively narrow range of propagation directions. A string of receivers in a vertical borehole was used to record the wavefield excited by perforation shots set off in a horizontal hole to induce hydraulic fracturing. The attenuation coefficient was represented as a quadratic polynomial of the polar and azimuthal angles, and the polynomial coefficients

	A $\times 10^{-3}$	B $\times 10^{-3}$	C $\times 10^{-3}$	D $\times 10^{-3}$	E $\times 10^{-3}$	F $\times 10^{-3}$
Stage 3	26.7 ± 2.0	–	-117.6 ± 21.9	-40.8 ± 8.6	–	49.4 ± 13.9
Stage 4	24.2 ± 1.2	–	-72.0 ± 14.4	-20.8 ± 4.4	–	24.9 ± 7.1
Stage 5	22.1 ± 1.6	–	–	-21.6 ± 6.7	–	27.5 ± 10.2
Stage 6	7.3 ± 0.9	–	-106.2 ± 14.9	–	–	163.6 ± 25.7
Stage 7	15.8 ± 0.7	–	107.5 ± 15.9	40.7 ± 21.5	–	-354.9 ± 60.8

Table 1. Inverted elements of the model vector and their standard deviations for all stages. The dashes indicate the coefficients rejected by the best-subset regression.

	A $\times 10^{-3}$	B $\times 10^{-3}$	C $\times 10^{-3}$	D $\times 10^{-3}$	E $\times 10^{-3}$	F $\times 10^{-3}$
Stage 3	26.5 ± 0.6	–	-116.4 ± 6.0	-40.0 ± 3.0	–	49.6 ± 6.7
Stage 4	24.1 ± 0.3	–	-70.2 ± 2.7	-20.3 ± 1.2	–	24.3 ± 2.6
Stage 5	22.0 ± 0.2	–	–	-21.5 ± 1.3	–	28.0 ± 2.6
Stage 6	7.3 ± 0.1	–	-106.2 ± 3.6	–	–	163.7 ± 6.1
Stage 7	15.8 ± 0.1	–	107.7 ± 2.7	40.7 ± 0.9	–	-355.3 ± 9.8

Table 2. Sensitivity of the inversion results to errors in the origin times. The standard deviations are computed by contaminating the origin times with 100 realizations of Gaussian noise that has a standard deviation of 20 time samples.

were estimated by applying the spectral-ratio method to pairs of traces. The data for each stage of perforation shots were processed separately, with the attenuation coefficient expanded around the corresponding "central ray." The inversion results show that taking anisotropy into account substantially improves fitting of the attenuation measurements. The angular variation of the attenuation coefficient is more pronounced in the vertical plane, so polar attenuation anisotropy is stronger than azimuthal anisotropy.

The mean value of the attenuation coefficient decreases with successive stages of hydraulic fracturing and stimulation. This could be due to the diffusion of stimulant fluids in the induced fractures, which stiffens the medium and makes it less attenuative. Microseismic monitoring can delineate the extent of the zones of fluid diffusion, which should help verify this hypothesis. Because the reservoir formation is made up mostly of shale, it is likely to exhibit intrinsic attenuation anisotropy, whose contribution may complicate analysis of the attenuation signature of hydraulic fracturing.

ACKNOWLEDGMENTS

We thank Shell E&P Company and EnCana for providing the data. We are grateful to Vladimir Grechka (Shell), Serge Shapiro (Free University of Berlin), and the members of the A(nisotropy)-Team of the Center for Wave Phenomena (CWP), Colorado School of Mines, for fruitful discussions. Support for this work was provided by the Consortium Project on Seismic Inverse Methods for Complex Structures at CWP and by the Research Partnership to Secure Energy for America (RPSEA).

References

Aster, R. C., B. Borchers, and C. H. Thurber, 2005, Parameter Estimation and Inverse Problems: Elsevier.

Barnes, C., 2010, Anisotropic anelastic full waveform inversion: Application to North Sea offset VSP data: 80th Annual International Meeting, SEG, Expanded Abstracts, 972–976.

Behura, J., and I. Tsvankin, 2009a, Estimation of interval anisotropic attenuation from reflection data: Geophysics, **74**, no.6, A69–74.

———, 2009b, Role of the inhomogeneity angle in anisotropic attenuation analysis: Geophysics, **74**, no.5, WB177–WB191.

Clark, R. A., P. M. Benson, A. J. Carter, and C. A. G. Moreno, 2009, Anisotropic P-wave attenuation measured from a multi-azimuth surface seismic reflection survey: Geophysical Prospecting, **57**, 835–845.

Dasios, A., T. Astin, and C. McCann, 2001, Compressional wave Q estimation from full-waveform sonic data: Geophysical Prospecting, **49**, 353–373.

De, G. S., D. F. Winterstein, and M. A. Meadows, 1994, Comparision of P- and S-wave velocities and Q's from VSP and sonic log data: Geophysics, **59**, 1512–1529.

Draper, N., and H. Smith, 1981, Applied Regression Analysis, Second ed.: John Wiley and Sons.

Grechka, V., and A. Duchkov, 2011, Narrow-angle representations of the phase and group velocities and their applications in anisotropic velocity-model building for microseismic monitoring: Geophysics, *(submitted for publication)*.

Maultzsch, S., M. Chapman, E. Liu, and X.-Y. Li, 2007, Modelling and analysis of attenuation anisotropy in multi-azimuth VSP data from Clair

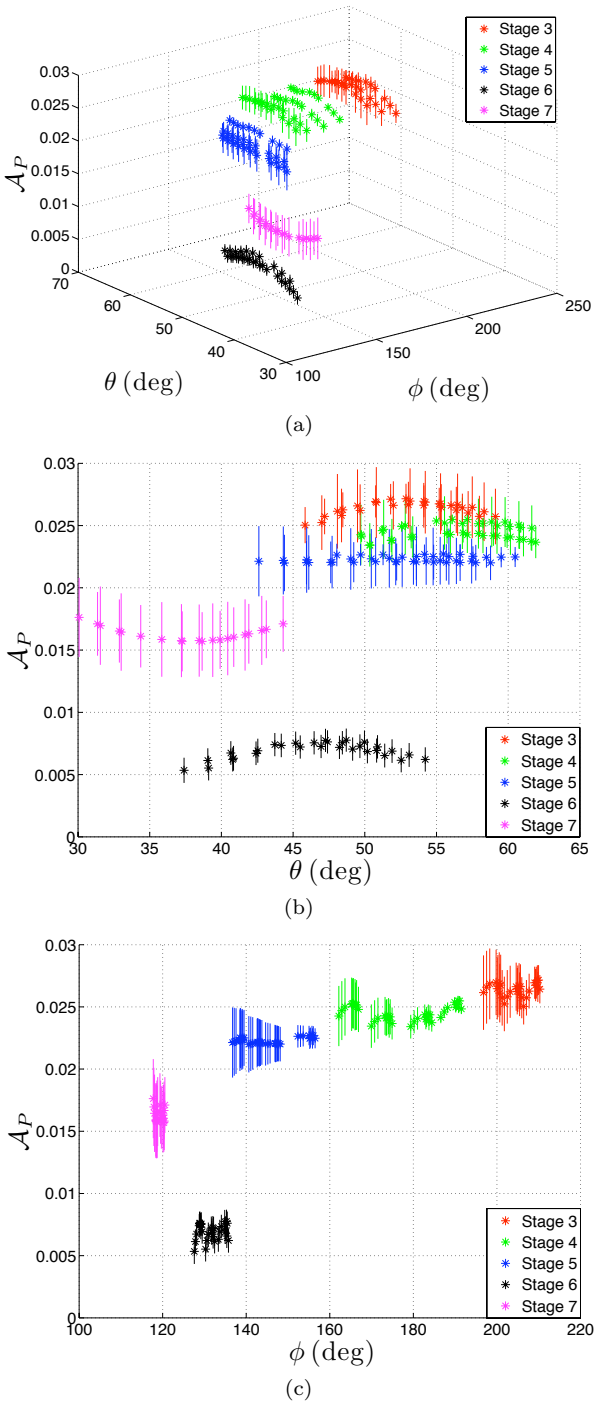

Figure 4. (a) P-wave attenuation coefficient (stars of different color) for all source-receiver pairs in spherical coordinates. (b) Variation of $\mathcal{A}_P$ with the polar angle obtained as the projection of plot (a) onto the [$\mathcal{A}_P$, θ]-plane. (c) Variation of $\mathcal{A}_P$ with the azimuthal angle.

field: Geophysical Prospecting, **55**, 627–642.

Quan, Y., and J. M. Harris, 1997, Seismic attenuation tomography using the frequency shift method: Geophysics, **62**, 895–905.

Scales, J. A., and A. Gersztenkorn, 1988, Robust methods in inverse theory: Inverse Problems, **4**, 1071–1091.

Shekar, B., and I. Tsvankin, 2010, Estimation of shear-wave interval attenuation from mode-converted data: 80th Annual International Meeting, SEG, Expanded Abstracts, 187–191.

Vasconcelos, I., and E. Jenner, 2005, Estimation of azimuthally varying attenuation from wide-azimuth P-wave data: 75th Annual International Meeting, SEG, Expanded Abstracts, 123–126.

Zhu, Y., and I. Tsvankin, 2006, Plane-wave propagation in attenuative transversely isotropic media: Geophysics, **71**, no.2, T17–T30.

———, 2007, Plane-wave attenuation anisotropy in orthorhombic media: Geophysics, **72**, no.1, D9–D19.

Zhu, Y., I. Tsvankin, P. Dewangan, and K. V. Wijk, 2007, Physical modeling and analysis of P-wave attenuation anisotropy in transversely isotropic media: Geophysics, **72**, no.1, D1–D7.